



$\alpha\beta$ T-cell receptor recognition of self-phosphatidylinositol presented by CD1b

Received for publication, September 6, 2022, and in revised form, December 21, 2022. Published, Papers in Press, December 29, 2022.
<https://doi.org/10.1016/j.jbc.2022.102849>

Rachel Farquhar¹, Ildiko Van Rhijn^{2,3}, D. Branch Moody², Jamie Rossjohn^{1,4,*}, and Adam Shahine^{1,*}

From the ¹Infection and Immunity Program and Department of Biochemistry and Molecular Biology, Biomedicine Discovery Institute, Monash University, Clayton, Victoria, Australia; ²Division of Rheumatology, Inflammation, and Immunity, Brigham and Women's Hospital and Harvard Medical School, Boston, Massachusetts, USA; ³Department of Infectious Diseases and Immunology, Faculty of Veterinary Medicine, Utrecht University, Utrecht, the Netherlands; ⁴Institute of Infection and Immunity, Cardiff University, School of Medicine, Cardiff, United Kingdom

Edited by Peter Cresswell

CD1 glycoproteins present lipid-based antigens to T-cell receptors (TCRs). A role for CD1b in T-cell-mediated autoreactivity was proposed when it was established that CD1b can present self-phospholipids with short alkyl chains (~C34) to T cells; however, the structural characteristics of this presentation and recognition are unclear. Here, we report the 1.9 Å resolution binary crystal structure of CD1b presenting a self-phosphatidylinositol-C34:1 and an endogenous scaffold lipid. Moreover, we also determined the 2.4 Å structure of CD1b-phosphatidylinositol complexed to an autoreactive $\alpha\beta$ TCR, BC8B. We show that the TCR docks above CD1b and directly contacts the presented antigen, selecting for both the phosphoinositol headgroup and glycerol neck region *via* antigen remodeling within CD1b and allowing lateral escape of the inositol moiety through a channel formed by the TCR α -chain. Furthermore, through alanine scanning mutagenesis and surface plasmon resonance, we identified key CD1b residues mediating this interaction, with Glu-80 abolishing TCR binding. We in addition define a role for both CD1b $\alpha 1$ and CD1b $\alpha 2$ molecular domains in modulating this interaction. These findings suggest that the BC8B TCR contacts both the presented phospholipid and the endogenous scaffold lipid *via* a dual mechanism of corecognition. Taken together, these data expand our understanding into the molecular mechanisms of CD1b-mediated T-cell autoreactivity.

While peptide antigen recognition forms the central dogma of classical T-cell-mediated adaptive immunity, the role of lipids as nonclassical antigens, presented by major histocompatibility complex class I-like molecules known as CD1, are emerging as new targets of protection and autoimmunity. CD1 mediated T-cell response to bacteria like *Mycobacterium tuberculosis* (1–14), and self-lipid antigens mediate autoreactivity and autoimmune disease *via* lipid activation (15–20), lipid-independent binding (21–25), and lipid-blocking mechanisms (26).

While mice only express CD1d, humans express CD1a, CD1b, CD1c, CD1d, and CD1e, which differ based on function, tissue localization, and sequence (27, 28). The mechanisms of antigen presentation by CD1d and recognition by natural killer T-cell receptors (NKT TCRs) are well established and involve direct TCR contact with the protruding headgroup moiety (29–32). However, emerging research has revealed recognition events that include mechanisms of direct CD1 protein recognition without recognition of carried lipid, cross-reactivity of many antigens based on their neck regions, and sideways approaches of TCRs to CD1 proteins (10, 19, 20, 24, 25, 33).

CD1b exhibits the largest antigen-binding cleft among isoforms in the CD1 family, which allows the molecule to accommodate a range of foreign- and self-lipid antigens with aliphatic hydrocarbon tails of up to C80 in length (10, 12, 19, 20, 34, 35). In some cases, a scaffold lipid is simultaneously bound inside CD1b along with the recognized antigen to stabilize its internal architecture (35–37). CD1b presents very long-chain foreign mycolyl lipids (38, 39) to germline-encoded mycolyl (GEM)-reactive and LDN5-like TCRs (10, 11, 40), with conserved TCR genes (41). In addition, CD1b presents self-lipid antigens, either cellular phospholipids or sphingolipids, to autoreactive $\alpha\beta$ and $\gamma\delta$ T cells (18–20).

Myeloid dendritic cells (42) can regulate CD1b expression and activate CD1b-restricted T cells, inducing an autoreactive immune response (27, 43). Furthermore, the presentation of self-phospholipid antigens by CD1b is possibly linked to oxidative stress upon phosphatidylglycerol (PG) presentation (20, 44), and both hyperlipidemia and protection against CD1b+ T-cell lymphoma upon presentation of phosphatidylethanolamine (45, 46).

To date, three CD1b-lipid antigen-TCR crystal structures have been solved (10, 19, 20). The mechanism of GEM $\alpha\beta$ TCR, GEM42, in recognition of CD1b presenting glucose 6-monomycolate (GMM), emphasizes how an invariant TCR contacts the protruding glycan epitope (47, 48). Other autoreactive T cells display diverse TCR expression and molecular modes of recognition of CD1b-lipid complexes (19, 20, 44).

An emerging classification system divides CD1b-TCR interactions into three categories: TCRs are highly specific for

* For correspondence: Adam Shahine, adam.shahine@monash.edu; Jamie Rossjohn, jamie.rossjohn@monash.edu.

TCR recognition of CD1b presenting PI

individual lipid structures, broadly reactive to a family of structurally related lipids or CD1b specific in a lipid-independent manner (19). For example, structural determination of CD1b in complex with autoreactive TCR PG90 (TRAV26-1/TRBV7-8) was highly specific for the phospholipid bound, whereas BC8B (TRAV9-2/TRBV6-2) could respond broadly to many glycerylphospholipids. This promiscuous recognition occurs because the TCR binds the neck region that is common to many phospholipid classes (19, 20). In both cases, the TCR directly recognized the amphipathic lipid headgroups exposed on the outer surface of CD1b, but not the scaffold lipid, which is typically seated beneath the antigenic lipid, distant from the TCR.

To further understand the molecular mechanisms underpinning CD1b-self-lipid antigen recognition, we sought to solve the structure of CD1b presenting a self-glycophospholipid in complex with an autoreactive $\alpha\beta$ TCR, BC8B. We determined the crystal structures of CD1b presenting self-phosphatidylinositol (CD1b-PI-C34:1) and CD1b-PI-C34:1-BC8B TCR and conducted alanine scanning mutagenesis on CD1b surface residues involved in BC8B TCR docking evaluated *via* surface plasmon resonance (SPR). Our findings support the model of broadly reactive $\alpha\beta$ TCR recognition of CD1b presenting self-antigens, highlight conserved residues necessary for CD1b-phospholipid recognition by BC8B, and provide direct evidence of dual recognition directed toward both the presented antigen and the scaffold lipid.

Results

Molecular mechanisms of CD1b presentation of cellular PI

Previous structural determination of the molecular mechanisms of PI-C33:0 presentation by CD1b involved the refolding

of CD1b expressed in *Escherichia coli*, which included the determination of artificially loaded detergent molecules within the binding pocket (35). In this study, we sought to determine the structure of CD1b exogenously loaded with cellular PI that contains two alkyl chains, C18 and C16:1, which combined have an overall unsaturation profile of C34:1. Cellular endogenous lipids were displaced from CD1b by first loading with lysosulfatide, and subsequently loaded with PI, and purified *via* anion exchange chromatography (Fig. 1A). Lipid loaded onto CD1b was validated by isoelectric focusing gel (Fig. 1B), before being crystallized, and the structure of CD1b-PI solved to a resolution of 1.9 Å (Fig. 2A and Table 1). The electron density for both PI acyl tails was clearly defined, with the C18:1 sn2 tail extending toward the base of the A' portal, and the C16:0 sn1 tail anchored in the C' portal (Fig. 2B). In addition, a single tube of electron density was observable with the T' and F' portals, corresponding to a single scaffold lipid of 31 carbons in length, where the lipid remains buried within the F' pocket (Fig. 2B).

The CD1b- β 2m complex reported here was expressed in human embryonic kidney 293S cells and exogenously loaded with PI-C34:1. This structure shares many similarities with the previously determined refolded CD1b-PI (PI-C33:0) structure (35), which overlays with an RMSD of 0.53 Å. Positioning of acyl tails and phosphate headgroup is highly similar across both structures. However, because of sn1 tail length differences by one carbon, PI-C33:0 penetrates deeper into the C' portal. The CD1b α 2 hinge region bends toward the PI-C34:1 headgroup, where the inositol moiety is anchored *via* hydrogen bond. This is not the case with PI-C33:0 (Fig. 2C), where the side chain of Gln152 faces in the opposite direction, away from PI-C33:0. This interaction between inositol and the outer surface of CD1b is notable because previously

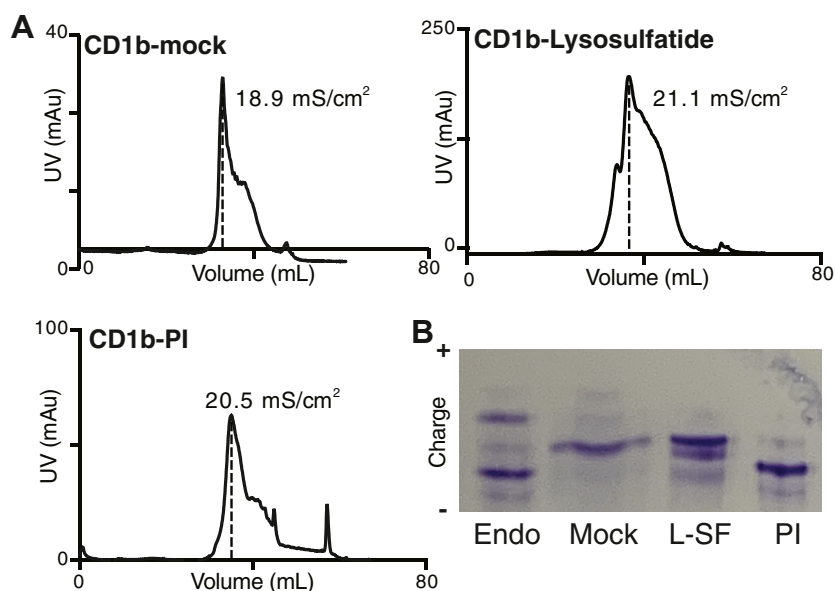


Figure 1. CD1b lipid loading validation. A, anion exchange chromatographs show CD1b treated with 0.5% tyloxapol (*mock*), CD1b loaded with lysosulfatide, and CD1b loaded with phosphatidylinositol (PI). The *dashed line* indicates peak elution at gradient level (mS/cm²). B, isoelectric focusing (IEF) analysis validated successful lipid loading of PI-C34:1 by CD1b. The IEF gel of CD1b shows complexes containing endogenous (endo) lipids, detergent-treated CD1b (*mock*), CD1b presenting lysosulfatide (L-SF), and CD1b presenting PI-C34:1 (PI). Lipid loading success was determined by charge separation of each protein on the gel. Migration of CD1b-PI-C34:1 protein toward the negative anode (-) indicates successful loading of the lipid of interest in comparison to CD1b presenting endogenous lipids and CD1b presenting L-SF.

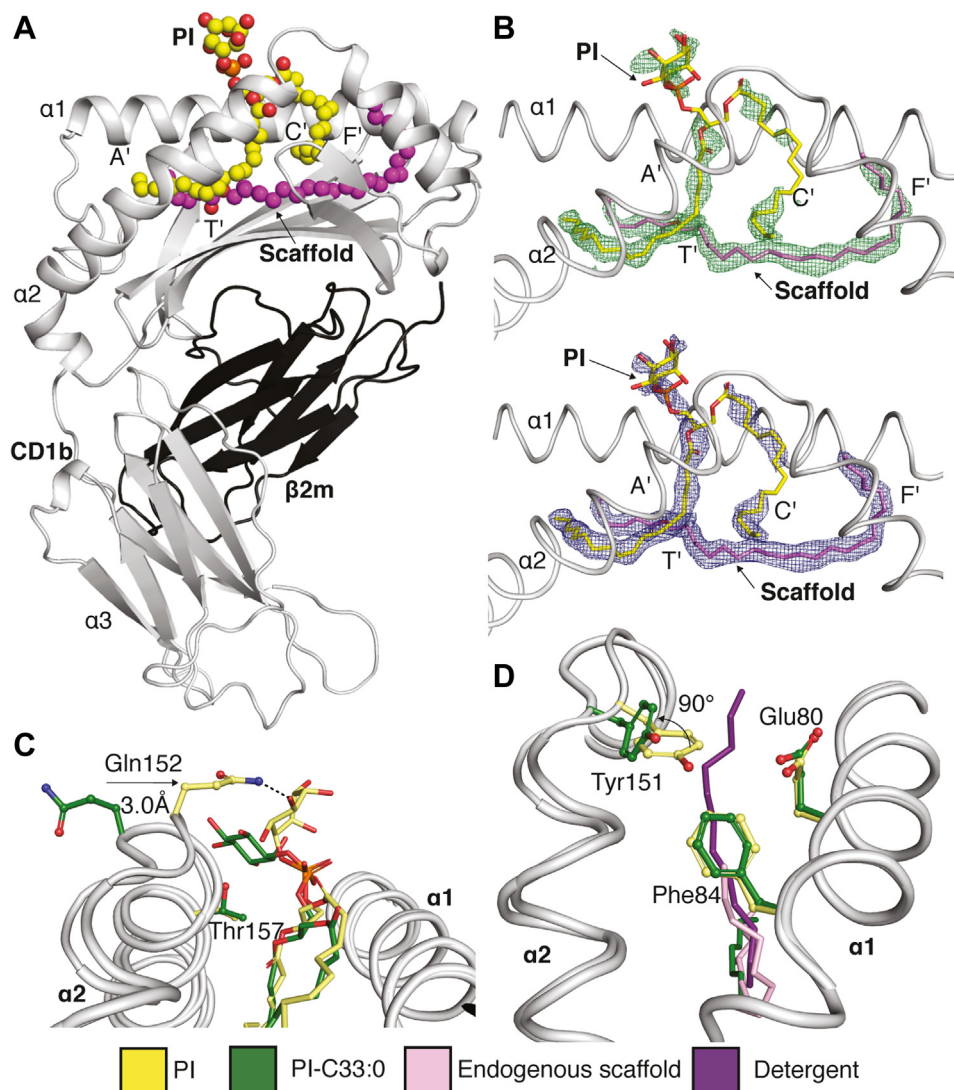


Figure 2. Presentation of PI-C34:1 by CD1b and comparison with refolded CD1b-PI-C33:0. A, structural overview of CD1b (gray), β 2m (black) presenting bound PI C34:1 PI-C34:1 (yellow) and scaffold wax ester lipid (purple) within the antigen-binding cleft. B, CD1b-PI-C34:1 binary crystal structure unbiased (green, upper) and refined (blue, lower) electron density maps of PI and scaffold lipids bound within the CD1b antigen-binding pocket. Unbiased and refined maps are contoured to 2.5σ and 0.8σ , respectively. C and D, structural comparison overlay between the binding clefts of CD1b presenting PI-C34:1 (CD1b-PI-C34:1, yellow) and refolded CD1b-PI-C33:0 (Protein Data Bank ID: 1GZP, green), with a focus on (C) the phospholipid antigen headgroups around the α 2 helix hinge region and (D) the buried F' pocket and overlay between scaffold (pink) and detergent (purple) molecules. Amino acids are represented as sticks, with directions of movement indicated by black arrows. Nitrogen, oxygen, and sulfur atoms are colored in blue, red, and orange, respectively. PI, phosphatidylinositol.

determined CD1b-phospholipid antigen structures show no significant contacts made between CD1b and the solvent-exposed headgroup (37).

The key differences between the positioning of CD1b-PI-C34:1 and CD1b-PI-C33:0 relates to the endogenous scaffold and detergent molecules positioned within the F' portal. The F' portal, which provides access of the antigen to the outer surface of CD1b, is capped by a Van der Waals (VDW) network among Glu80, Phe84, and Tyr151. The endogenous scaffold lipid is buried underneath the F' portal with the VDW network remaining intact. In the previously observed structure, detergent molecules disrupt the opening of the F' portal, with Tyr151 being displaced and rotated toward the solvent (Fig. 2D) (35). However, as the positioning of Tyr151 plays a role in TCR recognition (19), where dual the spacer lipid and

presented lipid is required for TCR contact, the movement of the positioning of Tyr151 appears to be dependent upon scaffold lipid length. Extension of the scaffold lipid to the outer surface of CD1b is unusual, as it normally lies beneath and beside, rather than above the antigenic lipid.

BC8B TCR docking onto CD1b-PI-C34:1

To ascertain the molecular mechanisms of CD1b-PI recognition, we produced the BC8B TCR and cocrystallized with CD1b-PI, with the ternary structure determined to a resolution of 2.4 \AA (Fig. 3A and Table 1). There is incomplete density for the solvent-exposed inositol ring and well-defined density for the phosphate moiety (Fig. 3B). Clear tubes of density are present for the sn1 and sn2 acyl tails and spacer lipid. Compared with the previously solved structure of

TCR recognition of CD1b presenting PI

Table 1
X-ray data collection and refinement statistics

Parameters	CD1b-PI	BC8B-CD1b-PI
Space group	P 21 21 21	P 1 21 1
Resolution range (Å)	46.39–1.90 (1.97–1.90)	41.13–2.40 (2.49–2.40)
Cell dimensions (Å, °)	$a = 57.82$, $b = 78.63$, and $c = 92.73$ $\alpha = \beta = \gamma = 90$	$a = 73.09$, $b = 65.43$, and $c = 101.58$ $\alpha = \gamma = 90$ and $\beta = 102.26$
Total no. of reflections	496,450 (31,344)	260,716 (26,509)
No. of unique reflections	33,822 (3316)	36,933 (3651)
Multiplicity	14.70 (14.70)	7.10 (6.90)
Completeness (%)	99.32 (98.66)	99.88 (99.86)
CC (1/2)	0.99 (0.73)	0.99 (0.87)
R_{pim} (%) ^a	6.20 (63.50)	5.90 (58.80)
Mean $I/\sigma(I)$ ^b	13.50 (2.10)	11.60 (2.20)
$R_{\text{factor}}/R_{\text{free}}$ (%) ^c	18.70/24.54	19.06/24.89
Nonhydrogen atoms	3585	6746
Macromolecules	3042	6247
Ligand	242	251
Solvent	301	248
Protein residues	380	821
Bond length (Å)	0.011	0.011
Bond angles (°)	1.22	1.27
Ramachandran plot		
Favored region (%)	98.94	97.10
Allowed region (%)	1.03	2.90
Outliers (%)	0.00	0.00
B -factors (Å ²)		
Average B -factors	33.41	61.12
Macromolecules	31.14	61.94
Ligands	54.81	81.40
Solvent	39.20	58.11
Protein Data Bank ID	8DV3	8DV4

Highest resolution shell is shown in parenthesis.

^a $R_{\text{pim}} = \sum_{\text{hkl}} [1/(N - 1)]^{1/2} \sum_i |I_{\text{hkl}, i} - \langle I_{\text{hkl}} \rangle| / \sum_{\text{hkl}} \langle I_{\text{hkl}} \rangle$.

^b $\sigma(I)$ is the estimated standard deviation of the integrated intensity (I).

^c $R_{\text{factor}} = \sum_{\text{hkl}} |F_o| - |F_c| / \sum_{\text{hkl}} |F_o|$ for all data except 5%, which were used for R_{free} calculation.

unliganded BC8B (Protein Data Bank [PDB] ID: 6CUH) (19), we observe negligible remodeling of the BC8B TCR upon docking onto CD1b-PI-C34:1, where unliganded and complexed TCRs overlay with an overall RMSD of 0.88 Å. However PI-C34:1 is lifted out of the antigen-binding pocket by the complementarity-determining regions (CDR) CDR1 α and CDR3 α loops of the variable domain of the BC8B TCR (BC8B-V α), resulting in an upward shift of the entire lipid by 4 Å (Fig. 3C).

The CDR1 α and CDR3 α specifically contact the sn1 acyl tail in the C' portal and the phosphate neck region, which connects the glyceryl unit to the inositol ring. The inositol moiety protrudes furthest from CD1b, and, instead of contacting the TCR, escapes laterally through a TCR escape channel formed between by CDR1 α and CDR3 α loops and situated above the A' roof of CD1b (Fig. 4, A and B). Thr28 α and Gln113 α stack against the inositol moiety as well as above by framework (FW) residue Asn2 α , where they partially angle the inositol for escape. Whilst not part of the lateral escape channel, additional hydrogen bonds are formed with the phosphate and glycerol moieties by Ser107 α and Tyr114 α , respectively, which lock in place the features shared across all phospholipid species (Fig. 4A).

The lateral escape channel was previously observed in the context of phosphatidylcholine (PC) recognition (19). This CD1b-PC-TCR example was proposed as a candidate mechanism by which TCRs could broadly recognize

phospholipids, if the class defining headgroup that is distal to the phosphate moiety escapes from the TCR-CD1 interface. However, evidence for escape of more than one headgroup was lacking, and it was unknown whether a larger phospholipid headgroup such as the inositol in PI would be recognized. For example TCR docking might be hindered or enhanced by steric or electrostatic interactions with the inositol ring in PI. Here, CDR3 α is more involved in recognition of PI compared with PC, with additional hydrogen bonds formed with Ser107 α and Tyr114 α against the phosphate and neck regions, respectively. Furthermore, because of the larger size of the inositol moiety compared with choline, the TCR α -chain FW and CDR1 α partially contact the inositol *via* VDW interactions, which in turn angle the headgroup to escape through the channel (Fig. 4A).

Interaction between CD1b and BC8B TCR is primarily mediated by the CDR3 β , which anchors the TCR above the F' pocket (Fig. 4, C and D and Table S1). Recognition of CD1b is largely mediated *via* a network of polar contacts formed between CD1b α 1 localized residues (Arg79, Glu80, Asp83, and Asp87) and BC8B TCR CDR3 α - β (Fig. 4C). Where BC8B-V β forms a complex network of interactions with CD1b α 1 domain with comparatively minor BC8B-V α engagement, BC8B-V α forms the majority of the contacts with the presented lipid *via* the CDR1 α and CDR3 α loops (Fig. 4A). This indicates that the two TCR chains have distinct yet harmonious roles in the recognition of CD1b-lipid complex: BC8B-V β anchors onto CD1b, whereas BC8B-V α determines phospholipid binding.

BC8B TCR recognizes the diacylated phospholipid in a nearly identical manner when compared with CD1b-PI-BC8B and CD1b-PC-BC8B (Fig. 4B). This was as expected because of the similarities in previously observed steady-state affinity measurements between CD1b-PC and CD1b-PI contacted by BC8B (19). Structurally, both lipids are presented in a near identical manner, with both phospho-headgroup moieties overlaying closely. Furthermore, the lateral escape channel formed between the CDR1 α and CDR3 α regions is conserved, with a distance of 9.1 Å between Thr28 α and Thr113 α (Fig. 4B) (19). Overall, these support the headgroup model by showing how two different headgroups can escape.

Dual antigenic PI-C34:1 and scaffold lipid contact by BC8B TCR Leu111 β

Comparing TCR-liganded and non-TCR-liganded structures, Leu111 β displaces Tyr151 on CD1b, resulting in a 90° rotation of its side chain (Fig. 4D). This rotation is observable in the presence of higher seated spacer lipids that move up within the F' portal, as compared with the previous CD1b-PI C33:0 binary structure. This rotation is also observed within the complex of BC8B-CD1b-PC; however, the scaffold lipid observed in the previously determined crystal structure was shorter (19), and as such, TCR contact was not observed.

Prior crystallographic data have demonstrated that CD1b-restricted TCRs specifically bind the antigenic lipid, while “ignoring” the buried scaffold lipid. Here, the CDR3 β region

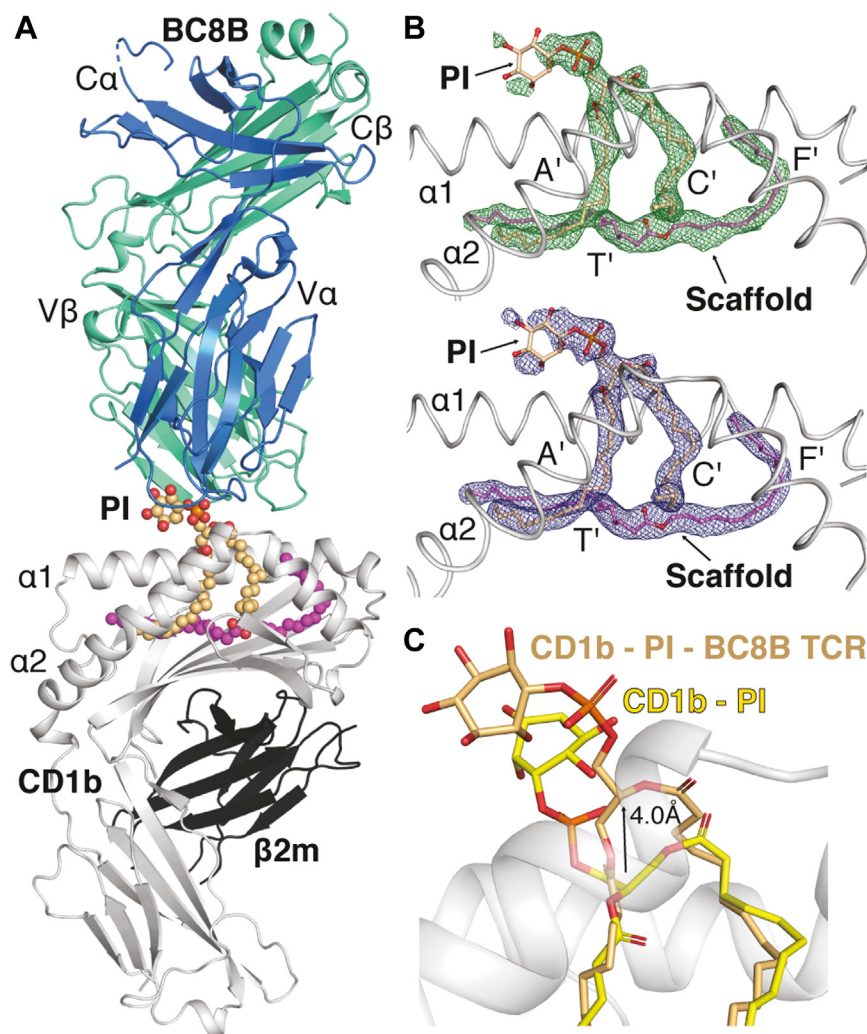


Figure 3. Overview of presentation of PI-C34:1 by CD1b to BC8B TCR and comparison with unliganded CD1b-PI-C34:1. *A*, ribbon diagram overview of CD1b (gray), $\beta 2m$ (black) presenting PI-C34:1 (light orange) and scaffold lipid (purple), and BC8B TCR (α -chain, blue; β -chain, green). Dashed lines on BC8B TCR α -chain indicate missing residues not visible in the electron density. *B*, CD1b-PI-C34:1-BC8B TCR ternary crystal structure unbiased (green, upper) and refined (blue, lower) electron density maps of PI and scaffold lipids bound within the CD1b antigen-binding pocket. Unbiased and refined maps are contoured to 2.5σ and 0.8σ , respectively. *C*, comparison of presentation of PI-C34:1 in the unliganded CD1b-PI-C34:1 (yellow) and CD1b-PI-C34:1-BC8B (orange) crystal structures. Arrow indicates upward directional movement of the PI antigen headgroup upon BC8B TCR docking. Oxygen and sulfur atoms are colored in red and orange, respectively. PI, phosphatidylinositol; TCR, T-cell receptor.

tightly locks onto CD1b above the F' pocket, *via* a network of polar contacts (Fig. 4C). This mode of contact allows Leu111 β of CDR3 β to penetrate the F' portal, where it contacts both the sn1 antigenic acyl tail at the entrance to the C' portal and the terminus of the C31 scaffold lipid at the F' portal opening.

This similar mechanism is observed in the previously determined complex of BC8B-CD1b-PC; however, the scaffold lipid does not protrude high enough through the F' portal to permit contacts with Leu111 β (Fig. S1, A and B) (19). In comparison, Leu110 β of the GEM42 TCR again penetrates the F' pocket of CD1b upon GMM presentation but favors contacts with the internal CD1b residue Phe84 (Fig. S1C) (10). A similar mechanism is observable for the CDR3 α Leu99 α residue of the human CD1d reactive NKT15 iNKT TCR, both of which do not involve dual lipid contacts (Fig. S1D) (29). Thus, unlike other CD1-reactive TCRs, hydrophobic bond-mediated dual recognition of the antigenic scaffold and the TCR CDR3 β is observed (Fig. 4D).

Energetic footprint reveals conserved role for Glu80 in TCR recognition

Alanine scanning mutagenesis was carried out to determine the impact of CD1b amino acid residues on BC8B TCR recognition. Specifically, we sought to determine the importance of contacts conserved across both CD1b-lipid-BC8B TCR structures. Based on contacts with the BC8B TCR, eight CD1b mutants containing endogenous lipids were produced, and steady-state binding kinetics toward BC8B TCR were analyzed *via* SPR (Fig. 5A).

The BC8B TCR exhibits a steady-state affinity of $13.6 \mu\text{M}$ for untreated CD1b-WT that is loaded with a mixture of endogenous (endo) cellular lipids sourced from the expression system. Previous SPR analysis determined that the BC8B TCR binds CD1b-endo and CD1b-PI with a similar affinity of 9.3 and $9.7 \mu\text{M}$, respectively (19). This outcome can be explained by the high content of phospholipids in endogenous CD1b and the ability of the TCR to cross-recognize many phospholipid

TCR recognition of CD1b presenting PI

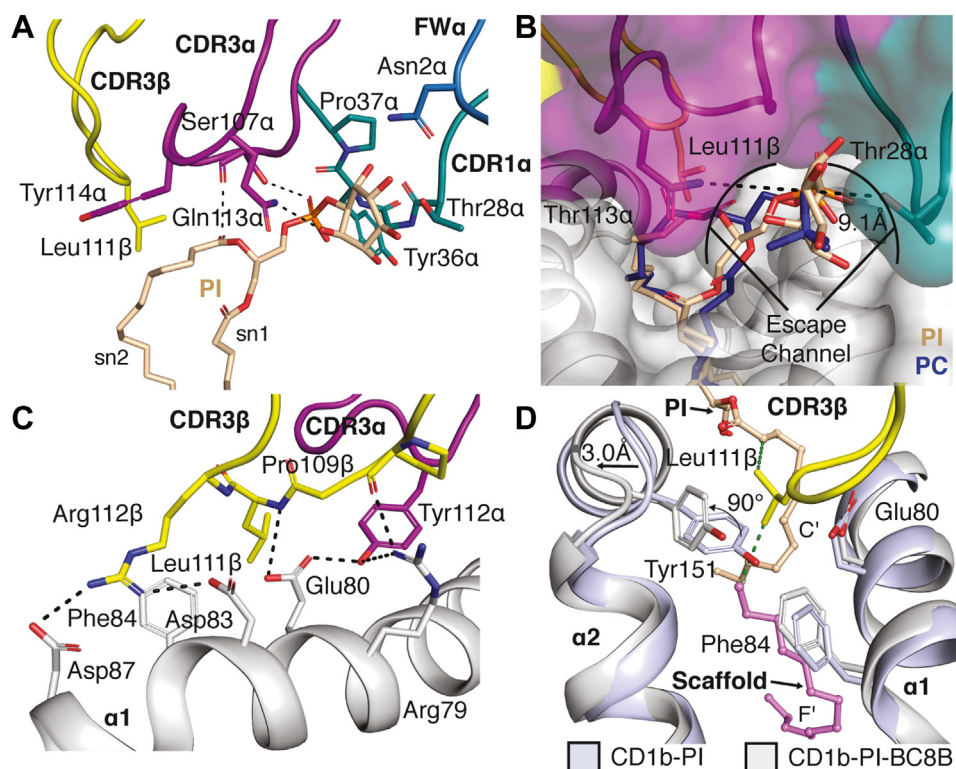


Figure 4. BC8B TCR recognition of PI-C34:1 and CD1b. *A*, BC8B TCR α -chain framework (FWa), CDR1 α (teal) and CDR3 α (purple), as well as the CDR3 β of BC8B TCR β -chain, contact the headgroup and neck region of PI-C34:1 via H-bonds (black dashed lines). Residues involved in lipid contacts are represented as sticks. *B*, comparison of lipid presentation in the ternary complexes CD1b-PC-BC8B (PDB ID: 6CUG) and CD1b-PI-C34:1-BC8B indicate that the escape channel (labeled) formed between the CDR1 α (teal) and CDR3 α (purple) by docking of BC8B on top of CD1b-lipid remains intact, and the escape channel diameter is conserved (black dashed line). Neck regions and phosphate groups of PC (blue) and PI-C34:1 (light orange) overlay directly, and both headgroups are accommodated. *C*, TCR CDR3 α and CDR3 β facilitate key contacts with CD1b along the CD1b α 1 region (gray). *D*, Leu111 β of the BC8B TCR β -chain (yellow) contacts both the PI-C34:1 and scaffold lipid simultaneously via hydrophobic interactions (green dashed lines). Black arrows between CD1b-PI-C34:1 before (blue) and after (gray) BC8B TCR binding indicate direction of movement. CDR, complementarity-determining region; PC, phosphatidylcholine; PI, phosphatidylinositol; TCR, T-cell receptor.

classes (20). As such, SPR analysis was conducted using CD1b-endo mutants for all affinity measurements. In this analysis, we found that none of the individual CD1b mutants enhanced BC8B TCR binding affinity compared with CD1b-WT. A change in affinity of CD1b-BC8B TCR was considered negligible if no fold change in steady-state affinity was observed (Gln152 and Glu156), moderate if threefold or less reduction occurred (Arg79 and Tyr151), significant if threefold to fivefold reduction (Val72 and Asp83) occurred, and critical if fivefold or more reduction occurred or abolishment of binding was seen (Glu80 and Ile154) (Fig. 5, A and B).

Tyr30 α of the TCR is wedged between CD1b residues Gln152 and Glu156 via VDW interactions; however, abolishment of these CD1b residues has no significant impact on BC8B TCR affinity (Fig. 5C). Arg79 forms hydrogen bonds with Pro109 β of the CDR3 β and Tyr112 α of the CDR3 α (Fig. 5D). Leu111 β displaces Tyr151 via VDW interactions, allowing for CDR3 β to penetrate the F' portal opening (Fig. 5C). A less than threefold reduction in binding was observed for Arg79Ala and Tyr151Ala, signifying moderate impact of this interaction of CD1b-BC8B binding. A threefold to fivefold reduction in binding affinity was recorded for Val72Ala and Asp83Ala on the α 1 helix. Val72 and Asp83 form VDW and salt bridge interactions with Tyr112 α on CDR3 α and Arg112 on CDR3 β ,

respectively, with Val72 contributing to the correct formation of the C' portal (Fig. 5D). Altering both residues suggests significant impact on both contacts with the key anchoring residue Arg112 β and correct formation of the C' portal for correct lipid presentation, respectively.

Glu80Ala and Ile154Ala on the α 1 and α 2 helices, respectively, recorded a greater than threefold to fivefold reduction in affinity. Whilst not forming key contacts with the BC8B TCR, Ile154 plays a critical role in antigenic lipid anchoring by forming the architecture of the CD1b C' portal, which is a CD1b-specific structure located beneath the α -helix, and is thought to allow escape of long lipids (35). Ile154 stacks against the sn2 acyl tail of PI, which anchors the presented antigen to allow for correct recognition by the BC8B TCR (Fig. 5C). These data show that anchoring and recognition of CD1b by the BC8B TCR is mediated via the α 1 helix of CD1b and the BC8B-V β interface. Glu80 forms a network of VDW and polar contacts with Leu111 and Arg110 of CDR3 β , and we found that alanine mutation of these residues abolished BC8B binding (Fig. 5D). This finding is consistent with previous CD1b-mutant studies where CD1b-lipid recognition is reduced or abolished by the Glu80Ala mutant in $\alpha\beta$ TCRs GEM42, PG90, and PG10 (20). This is due to the conserved role of Glu80 in hydrogen bond-mediated contact with the

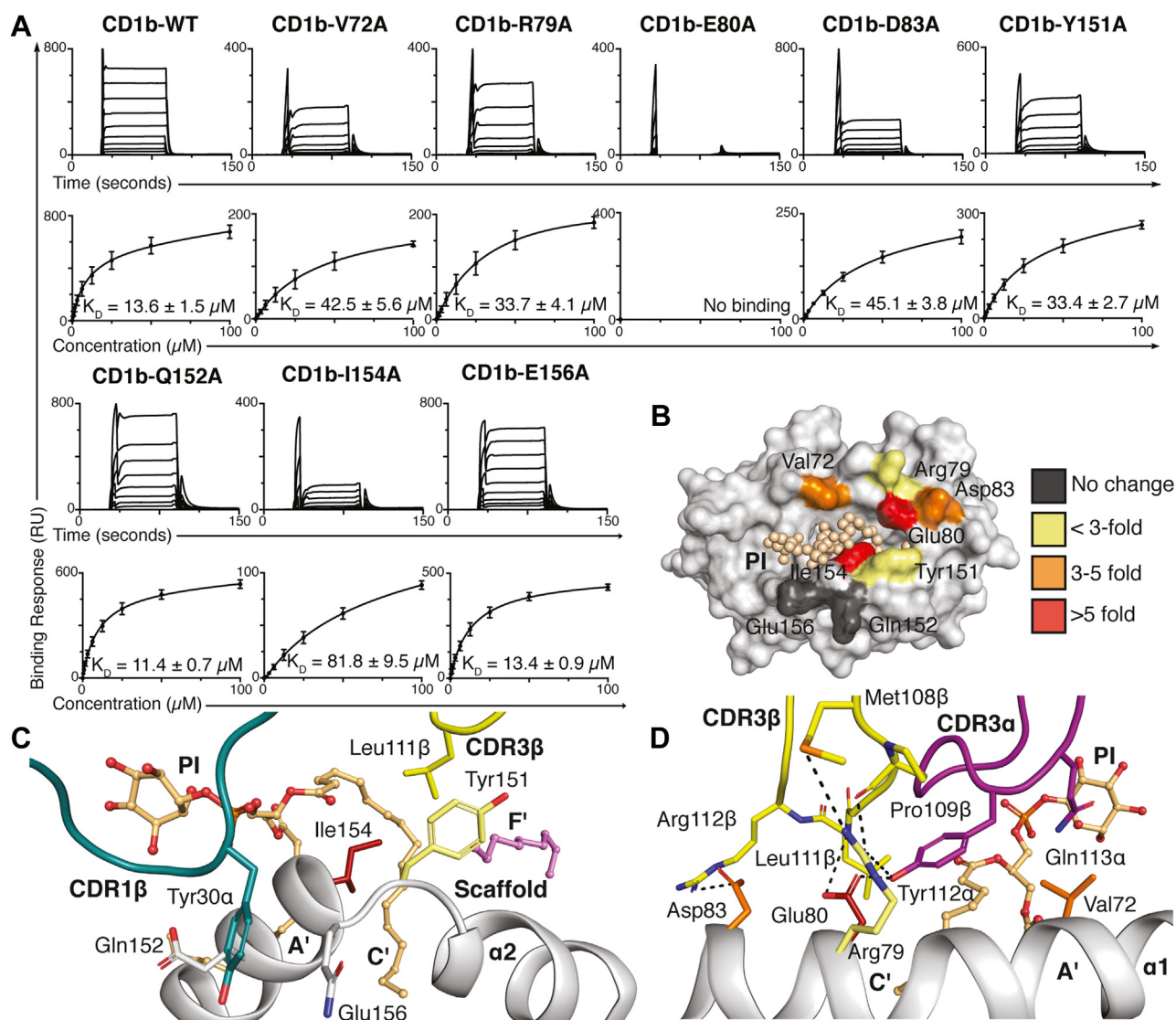


Figure 5. Surface plasmon resonance (SPR) steady-state affinities of BC8B interacting with CD1b alanine mutants of surface amino acids. A, BC8B binding against WT CD1b (CD1b-WT) alanine mutants was determined to establish the functional contact sites of the BC8B TCR and compared with interaction sites determined from structural studies. SPR experiments were conducted with two independent measurements in technical replicates, and steady state (K_D) measurements with error bars representing SEM are shown. GraphPad Prism software was used to generate sensorgrams (upper panel) and equilibrium curves (lower panel). B, the surface representation of CD1b (gray surface) with mutants was color coded based on the effect on binding affinity of the BC8B TCR: dark gray had no effect; yellow had less than threefold reduction; orange had between threefold and fivefold reduction; red indicates greater than fivefold reduction. C and D, mutated residues are color coded as B. Black dashes represent hydrogen bond formation. TCR CDR3 α , CDR1 β , and CDR3 β are colored in purple, teal, and yellow, respectively. Lipids PI and scaffold are colored in light orange and purple, respectively. Oxygen, nitrogen, and sulfur are colored red, blue, and orange, respectively. CDR, complementarity-determining region; PI, phosphatidylinositol; TCR, T-cell receptor.

TCR-V β (10, 19, 20) and its role in forming the F' portal opening. Taken together, through structural and functional analysis, it has been determined that residues on the surface of $\alpha 1$ domain of CD1b play a greater role than that of the $\alpha 2$ domain, with a denser cluster of residues with a critical role or a significant role in the binding of CD1b-BC8 TCR compared with previously characterized complexes with the GEM42 and PG90 TCRs (21, 20).

Defining the interface of BC8B TCR-CD1b and subsequent lipid headgroup mediation

This is the fourth CD1b-TCR ternary structure determined to date (10, 19, 20), advancing our understanding of the mechanisms governing lipid headgroup recognition by a

CD1b-reactive TCR. In all four cases, the $\alpha\beta$ TCR shows a small incident angle with CD1b to generate somewhat similar footprints on the distal surface CD1b in contrast with the recently observed $\gamma\delta$ TCRs that fail to recognize carried antigen because of their sideways binding to CD1a (21) and possibly CD1b (18). Whereas all four examples now increasingly point to TCR approach to the membrane distal surface of CD1b, the data can also distinguish between and explain the differing mechanisms of broadly reactive and antigen-specific CD1b-restricted TCRs (Fig. 6, A and B). In each case, TCR binding toward CD1b is dependent on direct contact and recognition of the antigenic lipid being presented (Fig. 6C). Furthermore, the newly determined BC8B TCR-CD1b-PI structure validates the broad model of antigenic recognition as hypothesized

TCR recognition of CD1b presenting PI

with the BC8B–CD1b–PC structure. Here, the TCR directly contacts the phosphate, glycerol, and sn1 acyl tail. These chemical elements can be considered common to the “neck” region of PI and PC as well as many other common diacylated phospholipids but are lacking in lysolipid and sphingolipid antigens. In contrast with this promiscuous mechanism of response to many types of phospholipids, other antigen-specific TCRs show high-affinity docking specific recognition of the particular antigenic polar headgroup, as observable with PG90 and GEM42 TCRs, which contact self-PG or foreign glucose monomycolate, respectively (Fig. 6A) (10, 20).

The BC8B α -chain docks centrally over the F' portal to contact the lipid antigen, and its footprint runs parallel across

the antigen-binding pocket of CD1b with a lateral escape channel formed by CDR1 α and CDR3 α encompassing the exposed lipid headgroup (Fig. 6B). As such, TCR α contributes the highest percentage of contacts with the antigenic headgroup, based on buried surface area (BSA) (Fig. 6D). Of the TCR α CDR loops, it is CDR3 α that coordinates most of the antigenic recognition surface, with BC8B CDR3 α contributing 51% of the total 77% BSA of TCR α against the presented phospholipid antigen. The remainder of the BSA against PI is determined by the FW and CDR3 β residues, which contribute at 7% and 15% of the binding surface, respectively (Fig. 6D).

In contrast, lipid antigen headgroup recognition is mediated equally by the α - and β -domains of antigen-specific TCRs,

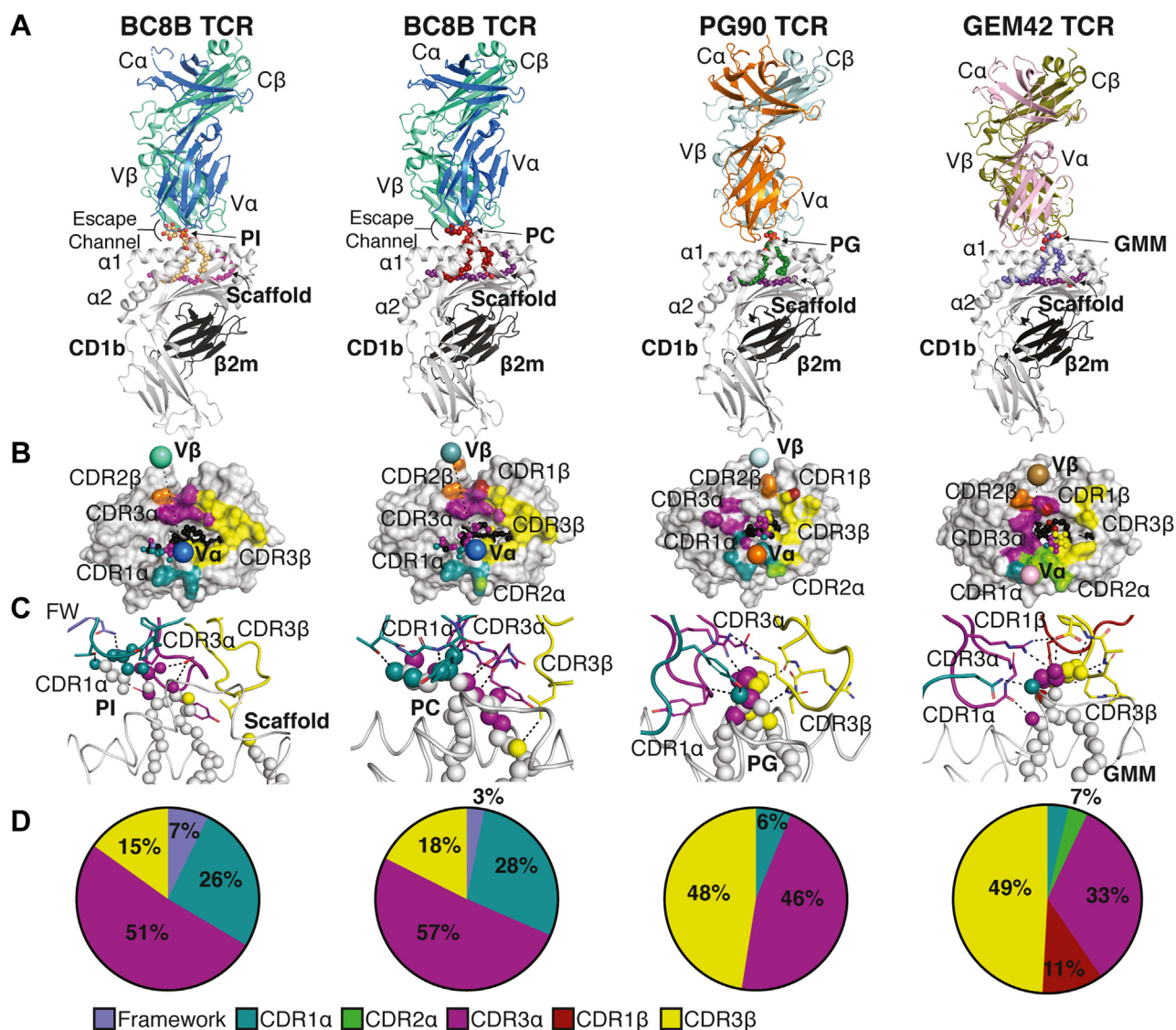


Figure 6. Comparison of CD1b–PI–C34:1–BC8B with ternary structures of CD1b–lipid complexes. *A*, ribbon diagrams of ternary complexes of CD1b presenting self (CD1b–PI–C34:1–BC8B, CD1b–PC–C34:1–BC8B, and CD1b–PG–PG90) and foreign lipids (CD1b–GMM–GEM42) for $\alpha\beta$ -TCR recognition. The BC8B TCR escape channels formed between the CDR1 α and CDR3 α are highlighted. *B*, spheres color coded to the respective α chain and β chains of the respective TCR complex representing the center of mass of the TCR. CD1b–PI–C34:1–BC8B (α -chain, blue; β -chain, green), CD1b–GMM–GEM42 (α -chain, brown; β -chain, pale pink), CD1b–PG–PG90 (α -chain, orange; β -chain, pale blue). *C*, $\alpha\beta$ -TCR contacts of lipid antigens presented by CD1b. CDR1 α (teal), CDR3 α (purple), CDR2 β (green), and CDR3 β (yellow) directly involved in lipid antigen recognition are represented as ribbons, with contact residues as sticks, and H-bonds (black dashed lines) with exposed head and neck regions of antigenic lipids. *D*, pie chart graphical representation of percentage buried surface area (%) between antigenic lipid headgroup and TCR framework (blue), CDR1 α (teal), CDR2 α (green), CDR3 α (purple), CDR1 β (red), and CDR3 β (yellow). CDR, complementarity-determining region; GEM, germline-encoded mycolyl; GMM, glucose 6-monomycolate; PI, phosphatidylinositol; TCR, T-cell receptor.

PG90 and GEM42. In both cases, ~50% of TCR docking is mediated by the CDR3 β , which play a role in both antigen headgroup and CD1b contact. Because of differences in PG90 and GEM42 gene usages, as well as differences in antigenic headgroup sizes between PG and GMM, the CDR3 α contact contributions differ amongst these TCRs (Fig. 6D). Antigen recognition is dependent on CDR3 α - β centric contacts by PG90 to completely sequester the PG headgroup and anchor onto CD1b, whereas the GEM42 TCR relies more heavily on the CDR1 β for antigenic anchoring (Fig. 6, C and D).

CD1b-reactive TCRs mediate antigen plasticity within the CD1b-binding groove

Remodeling of the lipids within the CD1b-binding pocket by TCR CDR is required to accommodate the final docking position and optimal antigen recognition. While the molecular mechanisms of broad and specific antigen recognition differ, antigenic rearrangement is consistently observable across all four CD1b–TCR crystal structures, resulting in partial elevation of the lipid from within the antigen-binding groove (Fig. 7).

While CDR rearrangement is minimal upon docking by the BC8B TCR, the seated antigen's position is elevated 3.6 to 4.0 Å within the A' and C' pockets. Furthermore, the CD1b α 2 hinge region is stabilized and rotated inward upon BC8B docking (Fig. 7, A and B). In contrast to this antigen lift mechanism, both the PG90 and GEM42 TCRs push the antigenic headgroup toward the F' pocket of CD1b by 4.3 to 6.1 Å, a shift that is accompanied by the CDR3 β surrounding and sequestering the headgroup (10, 20) (Fig. 7, C and D). In all four cases, TCR-induced remodeling moves the apparent terminus of the antigenic lipid by ~6 to 8 Å within the A' pocket, a change that is offset by the change in density corresponding to the bound scaffold lipids in the T' pocket, so that unliganded space within the cleft does not appear. This shift maintains the CD1b–lipid hydrophobic network for binding groove architectural integrity at the base of the A' pocket, despite the variable positioning of bound lipids (Fig. 7). This comparison demonstrates the plasticity of lipid placement within the antigen-binding pocket of CD1b, and that antigenic remodeling by the TCR is required for energetically optimized binding.

Discussion

Our understanding of CD1–lipid-mediated antigen recognition was originally derived from ternary crystal structures of NKT TCRs docking onto CD1d and hexosyl ceramides, whereby the TCR specifically recognizes CD1d and the hexose unit of the glycolipid (29, 48, 49). As this general model is expanded to amphipathic ligands other than glycolipids, as well as CD1 isoforms other than CD1d, additional chemical and structural features of TCR interaction with lipid antigens are emerging. TCRs can show extreme specificity for individual headgroups (40, 50), partial specificity for certain broad classes of lipids (19) or extreme ligand promiscuity for nearly all carried lipids (24, 25). As only the fourth solved ternary

structure of a CD1b–lipid–TCR complex, our work structurally validates a mechanism for TCR contact the shared neck regions common to many phospholipids, which occurs through escape of chemically diverse headgroups via a channel in the TCR. Furthermore, our data point to unexpected roles of scaffold lipid both in TCR contact and accommodating antigen movement within the cleft, as well as the beginnings of conserved approach angles and TCR footprint positions on CD1b.

Here, we show that BC8B CDR3 β contacts both exogenously loaded antigen and reaches down toward the F' portal to contact the endogenous scaffold lipid. Somewhat similar contacts of the CD1c autoreactive $\alpha\beta$ TCR 3C8 to the spacer lipid have been seen (25); however, the CD1b mechanism seen here is different in the sense that the TCR contacts both the spacer and the antigenic lipid. Our data inform and expand the hypothesis of Camacho *et al.* (9), who proposed in context of *M. tuberculosis* sulfolipid recognition that longer chain endogenous scaffold lipids (>C36) could possibly protrude beyond Tyr151 through the F' portal, potentially allowing for antigenic headgroup and scaffold lipid cocontact by the CDR3 of the TCR. While the long scaffold lipid observed here matched a length of 36 carbons based on electron density, the scaffold does not protrude from the F' portal, and instead, the TCR contact inside CD1b is demonstrated directly.

While the function of CD1b–phospholipid-reactive $\alpha\beta$ T cells is being elucidated in autoimmunity, the roles of self-reactive T cell such as BC8B are just beginning to be investigated. Furthermore, activation of CD1b+ autoreactive T cells after human CD1b transgenesis induced hyperlipidemia that leads to skin inflammation in mice (45, 46). Recent transcriptomic analysis revealed that CD1b gene upregulation indicates a positive prognostic score in localized prostate cancer patients (51). Furthermore, there is a marked increase in atypical mixed acyl tail PI species in prostate cancer tissue compared with benign epithelial tissue, which may act as both a potential biomarker for cancer prognosis as well as antigens for CD1b+ T cells (52). Alternatively, in the case of broadly reactive T cells such as BC8B, which do not selectively activate against a specific antigen, these T cells may play a role more in CD1b+ T-cell negative thymic selection, with CD1b+ T cells that dock *via* the antigen-specific model of corecognition playing a direct role in immunity (19).

Altogether, we have provided the molecular mechanisms of self-glycophospholipid presentation by CD1b and $\alpha\beta$ TCR recognition, expanded on our understanding of the molecular mechanisms of CD1b-restricted $\alpha\beta$ TCR autoreactivity. Conceptually, these data contribute to the gradually expanding structural characterization of TCR recognition of CD1b in defining distinct models of binding, with implications for the direct role of the endogenous scaffold lipid in T-cell-mediated immune activation. Future alanine scanning mutagenesis studies on TCR interface residues would be of benefit to further characterize mechanisms of docking onto CD1b. The next challenge would be to characterize the functional role of autoreactivity mediated by CD1b-reactive T cells and how

TCR recognition of CD1b presenting PI

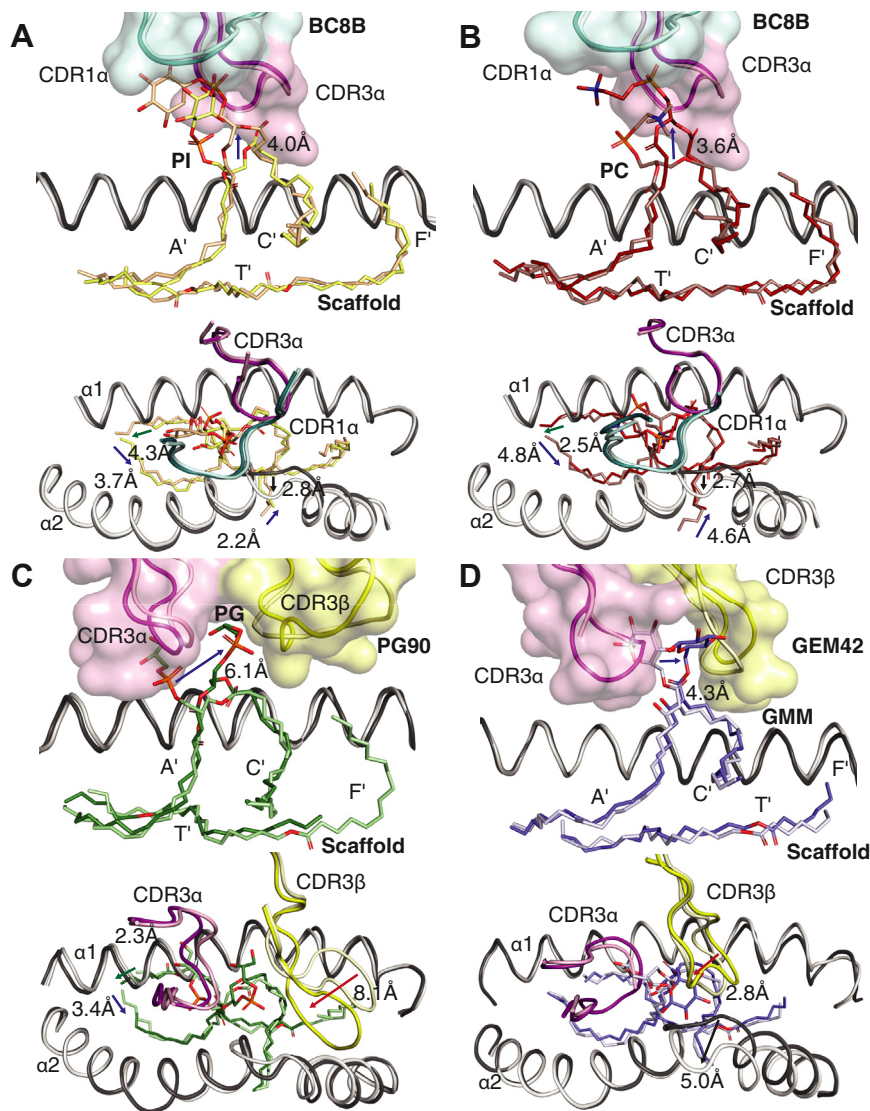


Figure 7. Comparison of lipid reorganization within the CD1b binding groove upon TCR docking. Side view structural overlays of CD1b–lipid binary complexes (*light*) and CD1b–TCR complexes (*dark*) of (A) CD1b–PI-32:1–BC8B (*yellow*), (B) CD1b–PC–BC8B (*red*), (C) CD1b–PG–PG90 (*green*), and (D) CD1b–GMM–GEM42 (*blue*). CD1b $\alpha 1$ and $\alpha 2$ helices (*gray*) as well as TCR CDR3 α (*purple*) and CDR3 β (*yellow*) are represented as *surfaces* (*upper*) and *ribbons* (*lower*), with lipid antigens and scaffold lipids represented as *sticks*. *Arrows* indicate direction and distance (in Å) of movement for CD1b (*black*), TCR (*red*), antigenic lipid (*blue*), and scaffold lipid (*green*). CDR, complementarity-determining region; PI, phosphatidylinositol; TCR, T-cell receptor.

these self-antigens mediated autoimmune responses in adaptive immunity.

Experimental procedures

Lipids

PI (catalog no.: 850142; C16:0/18:1) was purchased from Avanti Polar lipids. Lyso-sulfatide (lyso; catalog no.: 1904) was purchased from Matreya, LLC.

BC8B and CD1b protein production

Recombinant TCR BC8B was expressed and purified as previously described (19). Briefly, soluble domains of BC8B α and BC8B β were cloned into the pET30a vector, and expressed and refolded *via E. coli* inclusion bodies as well as purified by size-exclusion chromatography and HiTrap-Q HP anion exchange chromatography to homogeneity.

CD1b WT and alanine scanned mutants were solubly expressed in either *Trichoplusia ni* High Five insect cell line *via* baculovirus pFastBac dual transfection or *via* the mammalian adherent expression system using human embryonic kidney 293 S GnTI⁻. Soluble CD1b was purified to homogeneity by Ni²⁺-metal affinity chromatography to select for the N-terminal hexahistidine tag, followed by size-exclusion chromatography. Purity of BC8B and CD1b was assessed by SDS-PAGE.

Exogenous lipid loading into CD1b

Homogeneity of CD1b–lipid presentation was achieved by loading CD1b *via* a two-stage loading protocol previously described (19). Briefly, CD1b was incubated with a molar excess of lysosulfatide at pH = 4.0 and 0.5% tyloxapol (Merck; catalog no.: 25301-02-4) at room temperature overnight

followed by incubation at 37 °C for 60 min prior to purification *via* anion exchange chromatography. This was repeated using the CD1b–lysosulfatide sample with PI in a molar excess to obtain a homogeneous sample of CD1b–PI–C34:1. Lipid loading was validated by 4 to 6.5 pI gradient isoelectric focusing gel (Cytiva) and anion exchange chromatography. Proteins were buffer exchanged into 10 mM Tris (pH 8.0) and 150 mM NaCl for crystallographic and biophysical experiments.

Crystallization and structural determination

Crystals of CD1b–PI–C34:1 and CD1b–PI–C34:1–BC8B were grown *via* the hanging drop vapor diffusion method at 20 °C. Protein samples were concentrated to 5 mg ml⁻¹ and mixed with mother liquor at a ratio of 1:1, with a crystallization condition of 24% (w/v) PEG 3350, 2% ethylene glycol, 0.2 M sodium iodide for CD1b–PI–C34:1, and 24% (w/v) PEG 4000, 0.02 M Tris–HCl (pH 7.0), and 2% ethylene glycol for CD1b–PI–C34:1–BC8B. Crystals of CD1b–PI–C34:1 and CD1b–PI–C34:1–BC8B were soaked in a cryoprotectant of 10% (v/v) ethylene glycol + mother liquor and flash frozen in liquid nitrogen. Data were collected at the Australian Synchrotron at the MX2 beamline and made use of the Australian Cancer Research Foundation EIGER X 16M detector (Dectris) and Synchrotron Blu-Ice software, version 1.0 (53). Data were processed using XDS and scaled using AIMLESS as part of the CCP4i program suite (54). One complete dataset for each complex was collected. Crystal structures were solved by molecular replacement *via* Phaser as part of the Phenix program suite (55), with CD1b–PC (PDB ID: 6D64) and CD1b–PC–BC8B (PDB ID: 6CUG) used as models for CD1b–PI–C34:1 and CD1b–PI–C34:1–BC8B, respectively (19). Manual adjustment of each model was conducted in Coot (56), followed by maximum-likelihood refinement with Phenix-refine (55). Molecular representations of structures have been constructed using PyMOL (Shrodinger, <https://www.schrodinger.com/>), contacts were identified using the CONTACT program, and the center of mass was calculated using Areaimol within the CCP4i suite (54). Contact distance cutoffs were defined as 3.5 Å for hydrogen bonds, 4.5 Å for salt bridges, and 4.0 Å for VDW interactions.

SPR

SPR steady-state affinity measurements of BC8B against CD1b mutants V72A, R79A, E80A, D83A, Y151A, Q152A, I154A, and E156A containing endogenous lipids was conducted at 25 °C on the BIAcore 3000 instrument in 10 mM Tris–HCl (pH 8) and 150 mM NaCl supplemented with 0.5% (w/v) bovine serum albumin. Approximately 3000 RU of each monomer was coupled on the SA chip, with major histocompatibility complex class-I molecule H-2Db used for reference subtraction. Experiments were conducted as n = 2 with two technical duplicates. Steady-state affinity calculations using the 1:1 Langmuir binding model, data analysis, and visualization were generated using GraphPad 7.0.

Data availability

The crystallographic datasets generated and analyzed within the current study were deposited to the PDB under codes 8DV3 (crystal structure of CD1b presenting PI–C34:1) and 8DV4 (crystal structure of CD1b presenting PI–C34:1 to αβ TCR BC8B).

Supporting information—This article contains supporting information.

Author contributions—A. S. conceptualization; R. F., I. V. R., D. B. M., and A. S. methodology; R. F. and A. S. formal analysis; R. F. and A. S. investigation; I. V. R. and D. B. M. resources; R. F., J. R., and A. S. writing—original draft; R. F., I. V. R., D. B. M., J. R., and A. S. writing—review & editing; I. V. R., D. B. M., and J. R. supervision.

Funding and additional information—D. B. M. is supported by the National Institutes of Health grant (grant nos.: R01 AI049313 and R01 AR048632); J. R. is supported by a National Health and Medical Research Council investigator grant (grant no.: 2008981); A. S. is supported by an Australian ARC DECRA Fellowship (grant no.: DE210101031). The content is solely the responsibility of the authors and does not necessarily represent the official views of the National Institutes of Health.

Conflict of interest—D. B. M. consults for Enara and Pfizer. All other authors declare that they have no conflicts of interest with the contents of this article.

Abbreviations—The abbreviations used are: CDR, complementarity-determining region; FW, framework; GEM, germline-encoded mycolyl; GMM, glucose 6-monomycolate; NKT, natural killer TCR; PC, phosphatidylcholine; PDB, Protein Data Bank; PG, phosphatidylglycerol; PI, phosphatidylinositol; SPR, surface plasmon resonance; TCR, T-cell receptor; VDW, van der Waals.

References

- Moody, D., Ulrichs, T., Mühlecker, W., Young, D. C., Gurcha, S. S., Grant, E., *et al.* (2000) CD1c-mediated T-cell recognition of isoprenoid glycolipids in *Mycobacterium tuberculosis* infection. *Nature* **404**, 884–888
- Ulrichs, T., Moody, D. B., Grant, E., Kaufmann, S. H., and Porcelli, S. A. (2003) T-cell responses to CD1-presented lipid antigens in humans with *Mycobacterium tuberculosis* infection. *Infect. Immun.* **71**, 3076–3087
- Van Rhijn, I., Young, D. C., De Jong, A., Vazquez, J., Cheng, T. Y., Talekar, R., *et al.* (2009) CD1c bypasses lysosomes to present a lipopeptide antigen with 12 amino acids. *J. Exp. Med.* **206**, 1409–1422
- Zajonc, D. M., Crispin, M. D. M., Bowden, T. A., Young, D. C., Cheng, T. Y., Hu, J., *et al.* (2005) Molecular mechanism of lipopeptide presentation by CD1a. *Immunity* **22**, 209–219
- Moody, D. B., Young, D. C., Cheng, T. Y., Rosat, J. P., Roura-Mir, C., O'Connor, P. B., *et al.* (2004) T cell activation by lipopeptide antigens. *Science* **303**, 222–229
- Matsunaga, I., and Sugita, M. (2012) Mycoketide: a CD1c-presented antigen with important implications in mycobacterial infection. *Clin. Dev. Immunol.* **2012**, 981821
- Scharf, L., Nan-Shen, L., Hawk, A. J., Garzón, D., Zhang, T., Fox, L. M., *et al.* (2010) The 2.5 Å structure of CD1c in complex with a mycobacterial lipid reveals an open groove ideally suited for diverse antigen presentation. *Immunity* **33**, 853–862
- Beckman, E. M., Melián, A., Behar, S. M., Sieling, P. A., Chatterjee, D., Furlong, S. T., *et al.* (1996) CD1c restricts responses of mycobacteria-

TCR recognition of CD1b presenting PI

- specific T cells. Evidence for antigen presentation by a second member of the human CD1 family. *J. Immunol.* **157**, 2795–2803
9. Camacho, F., Moreno, E., Garcia-Alles, L. F., Chinae Santiago, G., Gil-leron, M., Vasquez, A., *et al.* (2020) A direct role for the CD1b endogenous spacer in the recognition of a Mycobacterium tuberculosis antigen by T-cell receptors. *Front. Immunol.* **11**, 566710
 10. Gras, S., Van Rhijn, I., Shahine, A., Cheng, T. Y., Bhati, M., Tan, L. L., *et al.* (2016) T cell receptor recognition of CD1b presenting a mycobacterial glycolipid. *Nat. Commun.* **7**, 13257
 11. Van Rhijn, I., Kasmar, A., de Jong, A., Gras, S., Bhati, M., Doorenspleet, M. E., *et al.* (2013) A conserved human T cell population targets mycobacterial antigens presented by CD1b. *Nat. Immunol.* **14**, 706–713
 12. Batuwangala, T., Shepherd, D., Gadola, S. D., Gibson, K. J. C., Zaccai, N. R., Fersht, A. R., *et al.* (2004) The crystal structure of human CD1b with a bound bacterial glycolipid. *J. Immunol.* **172**, 2382–2388
 13. Moody, D. B., Guy, M. R., Grant, E., Cheng, T. Y., Brenner, M. B., Besra, G. S., *et al.* (2000) CD1b-mediated T cell recognition of a glycolipid antigen generated from mycobacterial lipid and host carbohydrate during infection. *J. Exp. Med.* **192**, 965–976
 14. Roy, S., Ly, D., Li, N. S., Altman, J. D., Piccirilli, J. A., Moody, D. B., *et al.* (2014) Molecular basis of mycobacterial lipid antigen presentation by CD1c and its recognition by $\alpha\beta$ T cells. *Proc. Natl. Acad. Sci. U. S. A.* **111**, E4648–4657
 15. Melum, E., Jiang, X., Baker, K. D., Macedo, M. F., Fritsch, J., Dowds, C. M., *et al.* (2019) Control of CD1d-restricted antigen presentation and inflammation by sphingomyelin. *Nat. Immunol.* **20**, 1644–1655
 16. Gumperz, J. E., Roy, C., Makowska, A., Lum, D., Sugita, M., Podrebarac, T., *et al.* (2000) Murine CD1d-restricted T cell recognition of cellular lipids. *Immunity* **12**, 211–221
 17. Mansour, S., Tocheva, A. S., Cave-Ayland, C., Machelett, M. M., Sander, B., Lissin, N. M., *et al.* (2016) Cholesteryl esters stabilize human CD1c conformations for recognition by self-reactive T cells. *Proc. Natl. Acad. Sci. U. S. A.* **113**, E1266–1277
 18. Reijneveld, J. F., Ocampo, T., Shahine, A., Gully, B. S., Vantourout, P., Hayday, A. C., *et al.* (2020) Human $\gamma\delta$ T cells recognize CD1b by two distinct mechanisms. *Proc. Natl. Acad. Sci. U. S. A.* **117**, 22944–22952
 19. Shahine, A., Reinink, P., Reijneveld, J. F., Gras, S., Holzheimer, M., Cheng, T. Y., *et al.* (2019) A T-cell receptor escape channel allows broad T-cell response to CD1b and membrane phospholipids. *Nat. Commun.* **10**, 56
 20. Shahine, A., van Rhijn, I., Cheng, T. Y., Iwany, S., Gras, S., Moody, D. B., *et al.* (2017) A molecular basis of human T cell receptor autoreactivity toward self-phospholipids. *Sci. Immunol.* **2**, aao1384
 21. Wegrecki, M., Ocampo, T. A., Gunasighe, S. D., von Borstel, A., Tin, S. Y., Reijneveld, J. F., *et al.* (2022) Atypical sideways recognition of CD1a by autoreactive $\gamma\delta$ T cell receptors. *Nat. Commun.* **13**, 1–15
 22. Cotton, R. N., Cheng, T. Y., Wegrecki, M., Le Nours, J., Orgill, D. P., Pomahac, B., *et al.* (2021) Human skin is colonized by T cells that recognize CD1a independently of lipid. *J. Clin. Invest.* **131**, e140706
 23. Nicolai, S., Wegrecki, M., Cheng, T. Y., Bourgeois, E. A., Cotton, R. N., Mayfield, J. A., *et al.* (2020) Human T cell response to CD1a and contact dermatitis allergens in botanical extracts and commercial skin care products. *Sci. Immunol.* **5**, eaax5430
 24. Birkinshaw, R. W., Pellici, D., Cheng, T. Y., Keller, A. N., Sandoval-Romero, M., Gras, S., *et al.* (2015) $\alpha\beta$ T cell antigen receptor recognition of CD1a presenting self lipid ligands. *Nat. Immunol.* **16**, 258–266
 25. Wun, K. S., Reijneveld, J. F., Cheng, T. Y., Ladell, K., Uldrich, A. P., Le Nours, J., *et al.* (2018) T cell autoreactivity directed toward CD1c itself rather than toward carried self lipids. *Nat. Immunol.* **19**, 397–406
 26. Cotton, R. N., Wegrecki, M., Cheng, T. Y., Chen, Y. L., Veerapen, N., Le Nours, J., *et al.* (2021) CD1a selectively captures endogenous cellular lipids that broadly block T cell response. *J. Exp. Med.* **218**, e20202699fG
 27. Brigl, M., and Brenner, M. B. (2004) CD1: antigen presentation and T cell function. *Annu. Rev. Immunol.* **22**, 817–890
 28. Moody, D. B., and Cotton, R. (2017) Four pathways of CD1 antigen presentation to T cells. *Curr. Opin. Immunol.* **46**, 127–133
 29. Borg, N. A., Wun, K. S., Kjer-Nielsen, L., Wilce, M. C., Pellicci, D. G., Koh, R., *et al.* (2007) CD1d–lipid-antigen recognition by the semi-invariant NKT T-cell receptor. *Nature* **448**, 44–49
 30. Patel, O., Pellicci, D. G., Gras, S., Sandoval-Romero, M. L., Uldrich, A. P., Malleveay, T., *et al.* (2012) Recognition of CD1d-sulfatide mediated by a type II natural killer T cell antigen receptor. *Nat. Immunol.* **13**, 857–863
 31. Girardi, E., Maricic, I., Wang, J., Mac, T. T., Iyer, P., Kumar, V., *et al.* (2012) Type II natural killer T cells use features of both innate-like and conventional T cells to recognize sulfatide self antigens. *Nat. Immunol.* **13**, 851–856
 32. Rossjohn, J., Pellicci, D., Patel, O., Gapin, L., and Godfrey, D. I. (2012) Recognition of CD1d-restricted antigens by natural killer T cells. *Nat. Rev. Immunol.* **12**, 845–857
 33. Shahine, A., Wegrecki, M., and Le Nours, J. (2021) Novel molecular insights into human lipid-mediated T cell immunity. *Int. J. Mol. Sci.* **22**, 2617
 34. Garcia-Alles, L. F., Verslui, K., Maveyraud, L., Vallina, A. T., Sansano, S., Bello, N. F., *et al.* (2006) Endogenous phosphatidylcholine and a long spacer ligand stabilize the lipid-binding groove of CD1b. *EMBO J.* **25**, 3684–3692
 35. Gadola, S. D., Zaccai, N. R., Harlos, K., Shepherd, D., Castro-Palomino, J. C., Ritter, G., *et al.* (2002) Structure of human CD1b with bound ligands at 2.3 Å, a maze for alkyl chains. *Nat. Immunol.* **3**, 721–726
 36. Garcia-Alles, L. F., Collmann, A., Versluis, C., Lindner, B., Guiard, J., Maveyraud, L., *et al.* (2011) Structural reorganization of the antigen-binding groove of human CD1b for presentation of mycobacterial sulfolipids. *Proc. Natl. Acad. Sci. U. S. A.* **108**, 17755–17760
 37. Shahine, A. (2018) The intricacies of self-lipid antigen presentation by CD1b. *Mol. Immunol.* **104**, 27–36
 38. Beckman, E. M., Porcelli, S., Morita, C. T., Behar, S. M., Furlong, S. T., and Brenner, M. B. (1994) Recognition of a lipid antigen by CD1-restricted $\alpha\beta$ T cells. *Nature* **372**, 691–694
 39. Layre, E., Collmann, A., Bastian, M., Mariotti, S., Czaplicki, J., Prandi, J., *et al.* (2009) Mycolic acids constitute a scaffold for mycobacterial lipid antigens stimulating CD1-restricted T cells. *Chem. Biol.* **16**, 82–92
 40. Moody, D. B., Reinhold, B. B., Guy, M. R., Beckman, E. M., Frederique, D. E., Furlong, S. T., *et al.* (1997) Structural requirements for glycolipid antigen recognition by CD1b-restricted T cells. *Science* **278**, 283–286
 41. Reinink, P., Shahine, A., Gras, S., Cheng, T. Y., Farquhar, R., Lopez, K., *et al.* (2019) A TCR β -chain motif biases toward recognition of human CD1 proteins. *J. Immunol.* **203**, 3395–3406
 42. Roura-Mir, C., Wang, L., Cheng, T. Y., Matsunaga, I., Dascher, C. C., Peng, S. L., *et al.* (2005) Mycobacterium tuberculosis regulates CD1 antigen presentation pathways through TLR-2. *J. Immunol.* **175**, 1758–1766
 43. Leslie, D. S., Dascher, C. C., Cembrola, K., Townes, M. A., Hava, D. L., Hugendubler, L. C., *et al.* (2008) Serum lipids regulate dendritic cell CD1 expression and function. *Immunology* **125**, 289–301
 44. Van Rhijn, I., van Berlo, T., Hilmenyuk, T., Cheng, T. Y., Wolf, B. J., Tatituri, R. V., *et al.* (2016) Human autoreactive T cells recognize CD1b and phospholipids. *Proc. Natl. Acad. Sci. U. S. A.* **113**, 380–385
 45. Bagchi, S., He, Y., Zhang, H., Cao, L., Van Rhijn, I., Moody, D. B., *et al.* (2017) CD1b-autoreactive T cells contribute to hyperlipidemia-induced skin inflammation in mice. *J. Clin. Invest.* **127**, 2339–2352
 46. Bagchi, S., Li, S., and Wang, C.-R. (2016) CD1b-autoreactive T cells recognize phospholipid antigens and contribute to antitumor immunity against a CD1b(+) T cell lymphoma. *Oncoimmunology* **5**, e1213932
 47. Gras, S., van Rhijn, I., Shahine, A., and Le Nours, J. (2018) Molecular recognition of microbial lipid-based antigens by T cells. *Cell Mol. Life Sci.* **75**, 1623–1639
 48. Cotton, R. N., Shahine, A., Rossjohn, J., and Moody, D. B. (2018) Lipids hide or step aside for CD1-autoreactive T cell receptors. *Curr. Opin. Immunol.* **52**, 93–99
 49. Rossjohn, J., Gras, S., Miles, J. J., Turner, S. J., Godfrey, D. I., and McCluskey, J. (2015) T cell antigen receptor recognition of antigen-presenting molecules. *Annu. Rev. Immunol.* **33**, 169–200

50. Kawano, T., Cui, J., Yoezuka, Y., Toura, I., Kaneko, Y., Motoki, K., *et al.* (1997) CD1d-restricted and TCR-mediated activation of valpha14 NKT cells by glycosylceramides. *Science* **278**, 1626–1629
51. Lee, C. H., Chen, L. C., Yu, C. C., Lin, W. H., Lin, V. C., Huang, C. Y., *et al.* (2019) Prognostic value of CD1B in localised prostate cancer. *Int. J. Environ. Res. Public Health* **16**, 4723–4832
52. Goto, T., Terada, N., Inoue, T., Nakayama, K., Okada, Y., Yoshikawa, T., *et al.* (2014) The expression profile of phosphatidylinositol in high spatial resolution imaging mass spectrometry as a potential biomarker for prostate cancer. *PLoS One* **9**, e90242
53. Aragão, D., Aishima, J., Cherukuvada, H., Clarken, R., Clift, M., Cowieson, N. P., *et al.* (2018) MX2: A high-flux undulator microfocus beamline serving both the chemical and macromolecular crystallography communities at the Australian Synchrotron. *J. Synchrotron Radiat.* **25**, 885–891
54. Winn, M. D. B. C., Cowtan, K. D., Dodson, E. J., Emsley, P., Evans, P. R., Keegan, R. M., *et al.* (2011) Overview of the CCP4 suite and current developments. *Acta Crystallogr. Sect. D: Biol. Crystallogr.* **67**, 235–242
55. Adams, P. D., Afonine, P. V., Bunkóczi, G., Chen, V. B., Davis, I. W., Echols, N., *et al.* (2010) Phenix: a comprehensive Python-based system for macromolecular structure solution. *Acta Crystallogr. Sect. D: Biol. Crystallogr.* **66**, 213–221
56. Emsley, P., Lohkamp, B., Scott, W. G., and Cowtan, K. (2010) Features and development of Coot. *Acta Crystallogr. Sect. D: Biol. Crystallogr.* **66**, 486–501